Springer

KSME

Journal of Mechanical Science and Technology 26 (2) (2012) 345~352
www.springerlink.com/content/1738-494x
DOI 10.1007/s12206-011-1038-z

Application of the GTN model to predict the forming limit diagram of IF-Steel †

Mahmoud Abbasi[1,*], Mohammad A. Shafaat[1], Mostafa Ketabchi[1], Davoud F. Haghshenas[1] and Mohammad Abbasi[2]

[1]*Department of Mining and Metallurgy, Amirkabir University of Technology, Tehran, Iran*
[2]*Faculty of Aerospace Engineering, Sharif University of Technology, Tehran, Iran*

(Manuscript Received February 16, 2011; Revised August 25, 2011; Accepted October 14, 2011)

Abstract

Forming limit diagrams (FLDs) are extensively used in industries, particularly the auto industry. The establishment of these diagrams using a predictive approach can lead to reduction in both cost and time. In the present work, Gurson-Tvergaard-Needleman (GTN), a porosity-based model, was used to predict the FLD of an interstitial-free steel via finite element simulation. Optimum values of the GTN model were obtained by applying a response surface methodology (RSM) based on central composite design. Results show that RSM is a good method for an appropriate determination of the GTN model parameters, such as initial void volume fraction, effective void volume fraction, critical void volume fraction, and final void volume fraction. Furthermore, the experimental FLD of the specimen steel was considerably predicted using the obtained GTN model parameters.

Keywords: Ductile fracture; Forming limit diagram; GTN model; Response surface methodology

1. Introduction

A forming limit diagram (FLD) is a graph which depicts the major strains (ε_1) for all values of the minor strain (ε_2) at the onset of localized necking. However, because of scattering in the measured necking strains, a narrow band is normally utilized for necking evaluation [1].

The experimental determination of an FLD usually consumes a considerable amount of time and requires special equipment. Different analytical and numerical models have been used as alternative approaches to cope with these difficulties. Abbasi et al. [2] theoretically predicted the FLD of a tailor-welded blank which consists of interstitial-free (IF) steels using the Marciniak–Kuczynski (M-K) model. Moreover, they examined the effect of yield function on the predicted FLD. Aghaie-khafri et al. [3] presented an analytical method for calculating the FLDs of aluminum sheets based on the three deformation phases proposed by Jones and Gillis [4]. They reported that the combination of the Hosford yield function with the Voce hardening law resulted in a good-enough compatibility between experimental and predicted FLDs.

From an engineering perspective, the Gurson-Tvergaard-Needleman (GTN) approach is one of the well-known mesomechanical models for ductile fracture [5]. Brunet et al. [6] successfully applied a GTN model to determine the FLDs of Ni-based sheet metal and an aluminum alloy.

A survey of the literature shows that the correct identification of the GTN model parameters is a prerequisite for the successful analysis of ductile failure through the GTN damage model [5-8]. The main complexity of the GTN calibration model is the difficulty in direct measurement, or the identification of parameters through experimental tests. Consequently, inverse approaches have been utilized for evaluating the parameters [6]. In these approaches, identification procedures mostly utilize a non-linear least squares fitting of a dependent parameter, resulting from a finite element simulation (FEM), on the experimental specimen response (usually a tensile test). GTN best-fit parameters are obtained using the simulation results which show the closest match to the experiment.

Different approaches have been proposed for identifying GTN model parameters through inverse methods. For instance, Brunet et al. [9] investigated the FLDs of three aluminum sheets with a mild-steel sheet using the GTN model. Assuming the Tvergaard coefficients are fixed, the model parameters were adjusted by applying a uniaxial tensile test. In their work, the effective parameters were studied using the inverse method proposed by Fratini et al. [10].

Broggiato et al. [11] estimated the material parameters via image analysis. They illustrated that the load-displacement curve can be replaced with global quantities which result from measuring the specimen profile (processing of digital image) during loading. In this case, more data are available for cali-

† This paper was recommended for publication in revised form by Associate Editor Youngseog Lee

* Corresponding author. Tel.: +98 21 64542949, Fax.: +98 21 66405846
E-mail address: m.abbasi@aut.ac.ir

bration, leading to a high level of confidence and accuracy in the model parameter evaluation.

Identification of pertinent factors for the GTN damage model should be performed using a suitable experiment strategy design. Response surface methodology (RSM) simultaneously considers several factors at different levels. In addition, RSM gives a second-order polynomial model for the relationship among the various factors and responses based on central composite design (CCD) [12].

In the present work, GTN damage model parameters were identified through inverse method for an IF IF-steel using RSM. Different sets of GTN model parameter values were selected, and a simulation of tensile test was run for each set of values. To compare the simulated stress-strain and the experimental diagrams, four responses were selected as indicators. The four responses chosen were strain at maximum stress (R_1), maximum stress (R_2), strain at failure (R_3), and stress at failure (R_4). Finally, the proposed equations for the responses in terms of GTN model parameters were solved using genetic algorithm via Matlab software to find the unknown parameters. The identified GTN model parameters defined as the input data for ABAQUS software and FLD of the specimen steel were as predicted.

2. GTN model

According to the GTN model, local damage is caused by nucleation, growth, and subsequent coalescence of voids inside a material. These three mechanisms result in a resistance loss which, in turn, progressively leads to failure. The yield potential as an extension of the Gurson–Tvergaard model used in the context of plane stress for orthotropic materials [13] is represented as follows:

$$\Phi = \frac{q^2}{\sigma_y^2} + 2q_1 f^* \cosh(-\frac{3q_2 p}{2\sigma_y}) - (1 + q_3 f^{*2}) = 0 \quad (1)$$

where $f^*(f)$ is the damage function of the microvoid volume fraction or porosity (f). Tvergaard considered the constants $q_1 = 1.5$, $q_2 = 1$, and $q_3 = q_1^2$ instead of $q_1 = q_2 = q_3 = 1$, which was applied in the original Gurson's model [14]. The variable q represents the effective stress of the macroscopic Cauchy stress tensor, p denotes the hydrostatic pressure parameter, and σ_y describes the hardening of a fully dense matrix material. The damage model takes into account three main phases of the damage evolution which includes nucleation, growth, and coalescences as shown in Eq. (2) [13]:

$$df = df_N + df_G + df_C \,. \quad (2)$$

The nucleation of microvoids is expressed as follows [6]:

$$df_N = (\frac{f_N}{S_N\sqrt{2\pi}}).\exp(-\frac{(\bar{\varepsilon}^p - \varepsilon_N)^2}{2S_N^2}).d\bar{\varepsilon}^p \,. \quad (3)$$

Table 1. Mechanical properties and thickness of the specimen steel.

Y.S (MPa)	U.T.S (MPa)	Elongation (%)	n	K (MPa)	Thickness (mm)
160	280	48.5	0.23	435	1.1

The normal distribution of the nucleation strain has a standard deviation of S_N, mean value of ε_N and nucleate voids with a volume fraction of f_N. Growth of the present voids is based on the apparent volume change as well as the law of mass conservation and is expressed as follows [6]:

$$df_G = (1-f).(d\varepsilon_{11}^p + d\varepsilon_{22}^p + d\varepsilon_{33}^p) \,. \quad (4)$$

Finally, for the coalescence and final material failure, the modification of the yield condition is introduced through the function $f^*(f)$ specified by Tvergaard as follows [9]:

$$\begin{cases} f^* = f & f < f_c \\ f^* = f_c + \delta(f - f_c) & f \geq f_c \end{cases} \quad (5)$$

with:

$$\delta = \frac{(f_u^* - f_c)}{(f_f - f_c)}, \; f_u^* = \frac{1}{q_1} \,.$$

f_u^* is the ultimate value of f^* at ductile rupture, and f_c is the critical void volume fraction when the coalescence of microvoids occurs and the load bearing capability of the material sharply drops. Finally, f_f is the void volume fraction when the stress capability completely vanishes (final failure). From the above-mentioned relations, the identification of the GTN model parameters, which include initial void volume fraction (f_0), critical void volume fraction (f_c), final void volume fraction (f_f), effective void volume fraction (f_N), mean strain (ε_N) and standard deviation (S_N), is essential in analyzing the tearing behavior of ductile materials.

3. Materials and methods

3.1 Materials

IF-steel, due to its high ductility and formability, was selected as the test sample. IF-steel is a superior material choice in the automobile industry because of its properties [15]. Table 1 lists the mechanical properties of the IF-steel used for the experiment. The properties were obtained through tensile tests based on the ASTM-E8 Standard [16].

3.2 Tensile test

Tensile tests were performed using an Instron machine with a loading speed of 15 mm/min (loading capacity = 30 ton). Tensile test specimens were provided according to the ASTM-E8 standard [16]. The true stress-strain of the sample as well

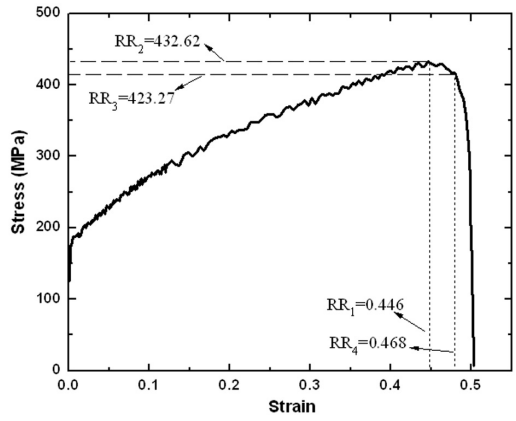

Fig. 1. Determination of responses from true stress-strain curve of the test steel.

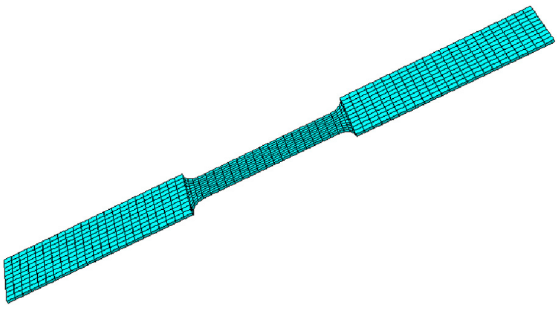

Fig. 2. Schematic representation of the meshed tensile-test specimen used in the simulations.

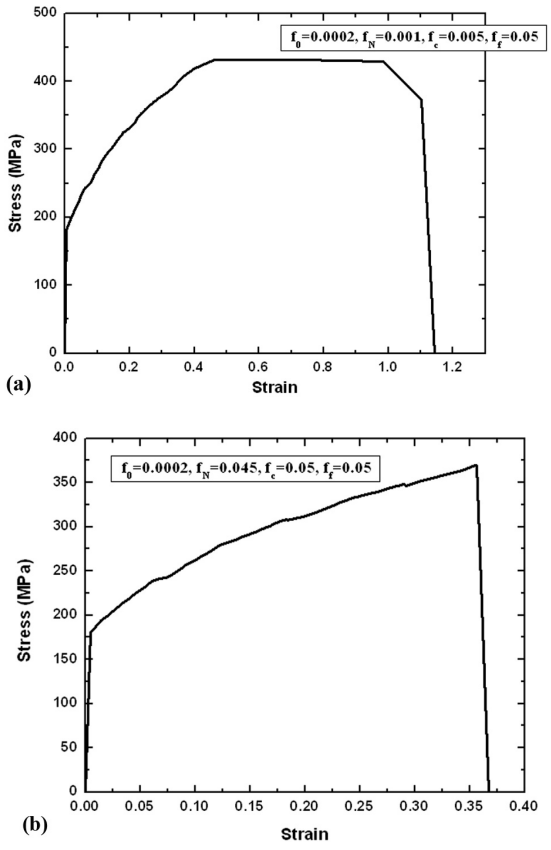

Fig. 3. True stress-strain curves obtained from the simulation results with the corresponding GTN model parameters.

as the four responses (RR_1, RR_2, RR_3, and RR_4) determined from the experiment are shown in Fig. 1.

Among the six major GTN damage model parameters—f_0, f_N, f_c, f_f, ε_N, and S_N—the last two variables were assumed constant ($\varepsilon_N = 0.1$, $S_N = 0.1$) [7, 17]. The procedure used in obtaining the domain change of the other factors is explained in detail in Ref. [18].

A CCD was adopted to study the other four factors at three levels and correspondingly different sets of parameter values were achieved. Each set of values was defined as the input data for ABAQUS, and the tensile test was simulated. From each run, four responses (maximum stress (R_2) and the corresponding strain (R_1) as well as strain (R_3) and corresponding stress (R_4) relating to the point where the stress falls abruptly) were determined. The responses correspond to the element wherein the tearing originally started (the point with $f = f_f$).

The tensile test simulation was performed using ABAQUS/Explicit [19]. The simulation parameters were defined according to the real experimental conditions. The material was assumed isotropic with elastic-plastic behavior which obeys the GTN model. Modeled parts were discretized using "continuum, 3D stress, 8-node linear brick, reduced integration" (C3D8R) elements. Although the effect of element size on the simulation results has been addressed by many researchers, this effect was ignored in the current work. The element size was considered as 3 mm, which is a normal value in the simulation of forming processes [20, 21].

Fig. 2 depicts the geometry of the test specimen and elements used in the simulation. In Fig. 3, two true stress-strain curves determined from simulation data with the corresponding GTN model parameters are shown. Fig. 3 shows that different values for the GTN model parameters result in various true stress-strain curves.

3.3 FLD test

The Hecker method [22] was used for determining the experimental FLD. This technique requires the use of different sample geometries to generate all possible strain and stress states.

Although this method can be implemented without using lubricants, the application of different lubricants results in various FLDs: the lower the friction coefficient, the higher the FLD level [22]. In the current research, oil with friction coefficient of 0.15 (between steel surfaces) was used as lubricant [23]. However, a comparison of experimental and simulation results on strain distribution by the authors has shown that 0.143 is a more valid value [24].

According to the Hecker method, one set of specimens includes material blanks that are cut in the required direction

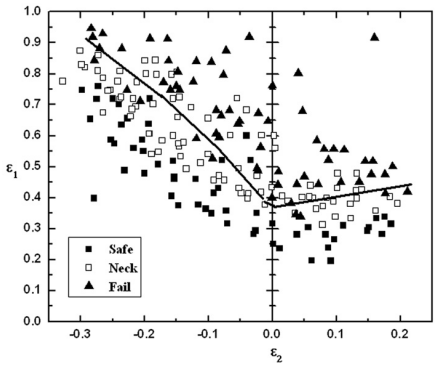

Fig. 4. Major and minor strains resulting from experiments as well as experimental FLD.

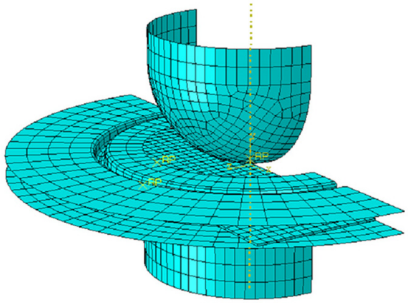

Fig. 5. Schematic representation of tools and blank modeled and meshed by ABAQUS.

with a length of 200 mm and different widths: 25 mm, 50 mm, 75 mm, 100 mm, 125 mm, 150 mm, 175 mm, and 200 mm. Each sample represents one strain path of the FLD.

A constant punch displacement speed (15 mm/min) was applied to deform each test specimen, and the blankholder was used to hold the specimen in place. The specimens were deformed until the first crack appeared on the sample. Prior to the onset of stamping, a circle-grid pattern with a diameter of 2.5 mm was electrochemically etched on the surfaces of all the specimens. The circles changed into ellipses of different sizes as the sheets deformed. The transverse and conjugate diameters of the ellipses were measured using a profile projector with an accuracy of ±1 μm. The major and minor strains were calculated in three distinct regions, namely, safe, necked, and fractured regions in all the blanks. The experimental FLD was developed by plotting the major and minor strains along the ordinate and abscissa, respectively. The curve which separated the fail region data from the rest was drawn. The results are presented in Fig. 4.

Simulation of the Hecker test was performed by applying ABAQUS software. Matrix, punch, and blank holder were considered as the rigid parts and the blank was assumed deformable. The parts were modeled according to the experiments. Punch speed during the simulations was set to 15 mm/min. The schematic geometry of the tools and the blank are presented in Fig. 5.

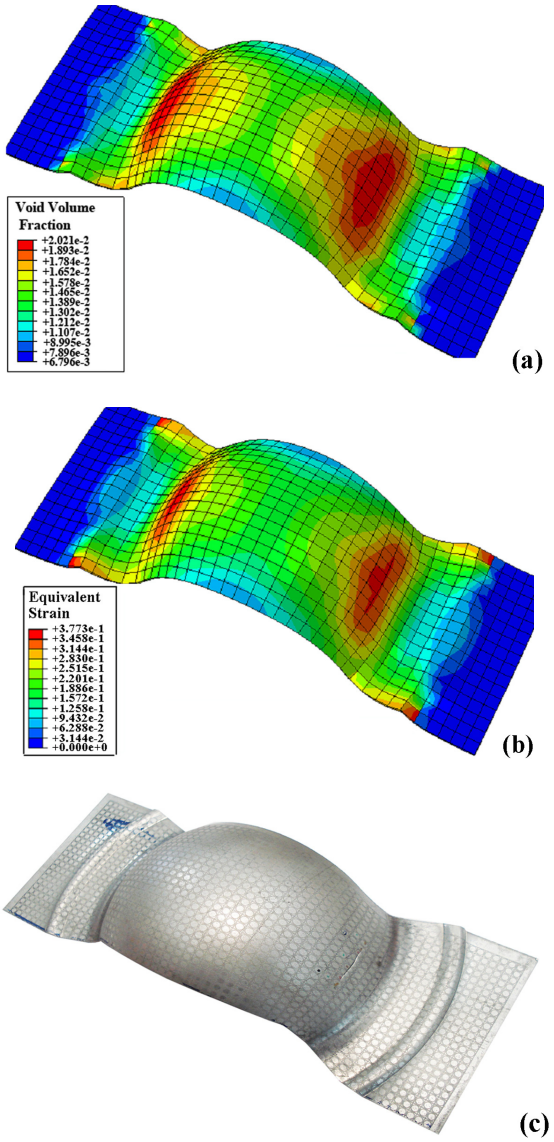

Fig. 6. Simulation results of (a) the void volume fraction; (b) the major strain distribution for the different elements of the specimen with 75 mm width; (c) figure of the sample which was torn during the experiment.

Coulomb's law was assumed between surface contacts during simulation, and 0.143 was used as friction coefficient. An elastic-plastic characteristic which obeyed porous metal plasticity was defined for the blank. Identified GTN model parameters were defined for software analysis, thereby simulating the forming process. All the blanks, with geometries according to the Hecker method, were formed until the final void volume fraction for an element was fulfilled.

Major and minor surface strains of an element in which $f = f_f$, were selected as the failure strains of the corresponding specimen. Figs. 6(a) and 6(b) illustrate the void volume fractions of the different elements and the corresponding major surface strains, respectively, when the critical condition ($f = f_f$) is satisfied. Moreover, the figure of the experimentally torn

Table 2. Central composite design (CCD) arrangement and responses.

Experiment number	Factors				Responses			
	f_0	f_N	f_C	f_f	R_1	R_2	R_3	R_4
1	0.0002	0.001	0.0050	0.050	0.46	431.83	1.11	373.56
2	0.0020	0.001	0.0050	0.050	0.49	426.82	0.49	426.80
3	0.0002	0.045	0.0050	0.050	0.046	221.71	0.046	221.70
4	0.0020	0.045	0.0050	0.050	0.039	211.76	0.055	173.00
5	0.0002	0.001	0.0500	0.050	0.51	431.51	1.36	417.70
6	0.0020	0.001	0.0500	0.050	0.45	429.36	1.28	402.70
7	0.0002	0.045	0.0500	0.050	0.35	369.70	0.35	369.70
8	0.0020	0.045	0.0500	0.050	0.19	300.35	0.18	300.35
9	0.0002	0.001	0.0050	0.200	0.51	431.51	1.14	411.00
10	0.0020	0.001	0.0050	0.200	0.45	429.36	0.82	402.30
11	0.0002	0.045	0.0050	0.200	0.104	238.56	0.18	215.00
12	0.0020	0.045	0.0050	0.200	0.30	320.74	0.36	283.00
13	0.0002	0.001	0.0500	0.200	0.45	431.66	1.46	419.00
14	0.0020	0.001	0.0500	0.200	0.49	429.09	1.23	409.60
15	0.0002	0.045	0.0500	0.200	0.31	330.20	0.37	316.00
16	0.0020	0.045	0.0500	0.200	0.28	320.26	0.40	302.60
17	0.0002	0.023	0.0275	0.125	0.41	391.29	0.52	285.00
18	0.0020	0.023	0.0275	0.125	0.35	369.16	0.46	290.00
19	0.0011	0.001	0.0275	0.125	0.46	430.61	1.43	405.00
20	0.0011	0.045	0.0275	0.125	0.19	316.42	0.26	240.00
21	0.0011	0.023	0.0050	0.125	0.18	301.20	0.24	270.00
22	0.0011	0.023	0.0500	0.125	0.44	407.74	0.77	335.00
23	0.0011	0.023	0.0275	0.050	0.33	371.72	0.33	370.00
24	0.0011	0.023	0.0275	0.200	0.43	394.16	0.62	300.00
25	0.0011	0.023	0.0275	0.125	0.38	374.75	0.49	275.00
26	0.0011	0.023	0.0275	0.125	0.39	375.00	0.49	275.50
27	0.0011	0.023	0.0275	0.125	0.42	406.00	0.52	360.00
28	0.0011	0.023	0.0275	0.125	0.40	377.92	0.47	330.00

specimen with the same width as the simulated ones is depicted in Fig. 6(c). Based on the data in Fig. 6, there is a good compatibility between the simulation and the experiment in the prediction of the tearing site. After determination of the major and minor failure strains of different specimens, the FLD of the studied steel was predicted.

3.4 Experimental design for RSM

For the CCD adopted to study the four factors at three levels each, 28 simulation tensile test runs were generated based on the principle of RSM using MINITAB Release 15. The levels employed for the different factors, which were based on CCD as well as the corresponding responses obtained from each run, are listed in Table 2.

The quadratic polynomial regression model was chosen for predicting the response variable in terms of the four independent variables [12]:

$$Y = b_0 + \sum_{i=1}^{4} b_i X_i + \sum_{i=1}^{4} b_{ii} X_i^2 + \sum_{i=1}^{3} \sum_{j=i+1}^{4} b_{ij} X_i X_j \ . \quad (6)$$

In Eq. (6), Y is the response variable (i.e., R_1, R_2, R_3, and R_4); b_0, b_i, b_{ii}, and b_{ij} are the coefficients of the intercept, linear, quadratic, and interaction terms, respectively; and X_i and X_j represent the four independent variables (i.e., f_0, f_N, f_c, and f_f). The simulations were performed using two replicates in random order to avoid systematic bias. The statistical significance of the full predicted quadratic models was evaluated using ANOVA. The significance and the magnitude of the effects of each variable and all their possible linear and quadratic interactions on the response variables were also determined. Unless otherwise stated, the significance level employed in the analysis was 10% ($p < 0.1$). Finally, the models were simultaneously solved to determine the optimum values using genetic algorithm method through Matlab software [25].

Table 3. ANOVA of the responses.

	df				SS				MS				P-values			
	R_1	R_2	R_3	R_4	R_1	R_2	R_3	R_4	R_1	R_2	R_3	R_4	R_1	R_2	R_3	R_4
Total	27	27	27	27	0.54	122519	4.98	142584								
Regression	14	14	14	14	0.43	116026	4.85	129868	0.035	8287.5	0.35	9276.3	0.00	0.00	0.00	0.00
Residual error	13	13	13	13	0.04	6493	0.13	12716	0.003	499.5	0.01	978.2				
Lack of fit	10	10	10	10	0.04	5807	0.12	7401	0.004	580.7	0.013	740.1	0.17	0.42	0.2	0.9
Pure error	3	3	3	3	0.007	686	0.001	5315	0.0002	228.7	0.001	1771.7				
R^2 (%)	92.0	94.7	97.4	91.0												

Table 4. Values of regression coefficients calculated for the responses.

Independent factor	Regression coefficient				Standard error				P-value			
	R_1	R_2	R_3	R_4	R_1	R_2	R_3	R_4	R_1	R_2	R_3	R_4
Constant	0.5	418	0.7	495	0.1	35	0.2	50	0.00	0.00	0.00	0.00
Linear												
f_0	-60.6	-9804	-47.9	30624	104.9	40859	181.1	57179	0.57	0.81	0.79	0.60
f_N	-7.7	-4677	-49.4	-7293	3.8	1476	6.5	2065	0.05	0.00	0.00	0.00
f_c	7.7	3547	17.6	399	4.2	1634	7.2	2287	0.07	0.05	0.03	0.86
f_f	-1.0	-178	4.6	-1593	1.6	640	2.8	896	0.54	0.79	0.13	0.09
Quadratic												
$f_0.f_0$	22944.0	1416778	-65852.6	-197452	44108.3	17179614	76142.5	240411	0.61	0.94	0.40	0.43
$f_N.f_N$	-76.8	-11493	618.1	39269	73.8	28751	127.4	40234	0.10	0.70	0.00	0.35
$f_c.f_c$	-103.6	-48607	-80.7	-1963	70.6	27487	121.8	38466	0.17	0.08	0.52	0.96
$f_f.f_f$	4.0	687	-12.6	5601	6.4	2474	11.0	3462	0.54	0.79	0.27	0.09
Interactive												
$f_0.f_N$	471.1	203021	3977.3	102431	724.5	282186	1250.7	394892	0.53	0.48	0.00	0.80
$f_0.f_c$	-748.3	-276472	808.6	-169599	708.4	275915	1222.9	386117	0.31	0.33	0.52	0.67
$f_0.f_f$	186.8	86558	170.4	104028	212.5	82775	366.9	115835	0.39	0.31	0.65	0.38
$f_N.f_c$	62.6	33476	-178.0	45032	29.0	11287	50.0	15796	0.05	0. 01	0.00	0.01
$f_N.f_f$	19.2	6199	8.5	5559	8.7	3386	15.0	4739	0.46	0.09	0.58	0.26
$f_c.f_f$	-5.7	-3269	-20.5	-1609	8.5	3311	14.7	4633	0.51	0.34	0.18	0.73

4. Results and discussion

4.1 Model fitting

Table 2 lists the values of four responses (R_1, R_2, R_3, and R_4) at each of the 28 combinations of the factor levels. The results of the ANOVA are presented in Table 3. The low p values for the regression ($P < 0.01$) and the fact that the lack of fit of the model was not significant ($P > 0.1$) indicate the suitability of the model.

The values of the regression coefficients are presented in Table 4. Both the linear f_N and f_c and interactive f_Nf_c terms are significant in the case of R_1, R_2, and R_3. For R_4, the linear f_N and f_f terms and the quadratic f_f term were significant. Additionally, f_0 was statistically insignificant in all responses. Based on the regression coefficients calculated for the responses (Table 4), the polynomial regression model equations, which fitted higher than 90% of the variation in the data, were proposed as follows:

$$R_1 = 0.47 - 4.05 f_N + 0.42 f_c - 93.08 {f_N}^2 + 62.63 f_N f_c \quad (7)$$

$$R_2 = 414.6 - 4207.3 f_N + 2875.3 f_c - 49358.7 {f_c}^2 + 33475.6 f_N f_c \quad (8)$$

$$R_3 = 0.85 - 33.14 f_N + 11.47 f_c + 383.2 {f_N}^2 - 178.03 f_N f_c \quad (9)$$

$$R_4 = 476.4 - 3440.3 f_N - 1457 f_f + 5848.4 {f_f}^2 . \quad (10)$$

4.2 Optimization of GTN damage model parameters

Using the proposed second order polynomial equations Eqs. (7) to (10), the optimum parameters using genetic algorithm were determined. The determined parameters and the corresponding stress-strain curve are shown in Table 5 and Fig. 7, respectively. The experimental stress-strain curve is also de-

Table 5. Optimized values of the evaluated parameters.

f_0	f_N	f_c	f_f
0.0002	0.0106	0.0134	0.02163

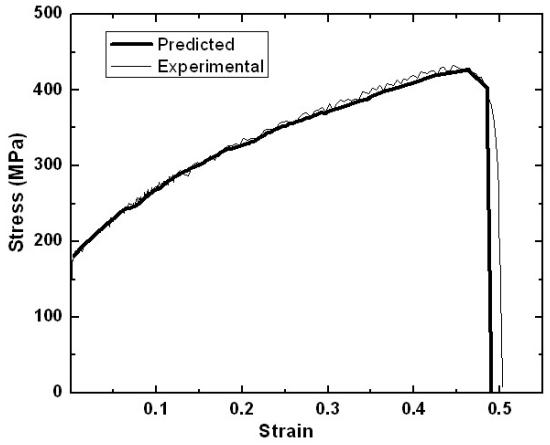

Fig. 7. Comparison between the experimental true stress-strain and the predicted curves obtained using the optimized values of the GTN damage model parameters.

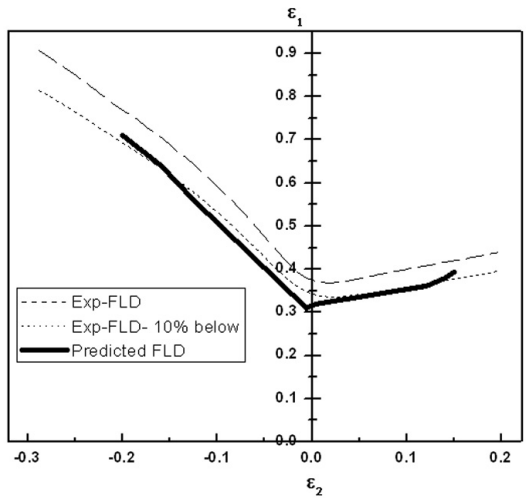

Fig. 8. Comparison among different FLDs obtained via experiments and prediction.

picted in Fig. 7 for comparison. As illustrated in Fig. 7, the simulated curve predicts the experimental result very well, especially prior to the point where the stress falls abruptly. More information about the utilization of genetic algorithm in finding optimum values of GTN model parameters can be found in Ref. [18].

4.3 Comparison between experimental and predicted FLDs

Fig. 8 shows the FLDs resulting from experiments (EXP-FLD) and the simulation runs (Predicted FLD). The EXP-FLD separates the fail strain data from the neck strain data. The region above the experimental curve (Exp-FLD) is considered unsafe for any particular deformation mode. This region indicates that fracture is inevitable. However, for strain combinations under the curve, the potential of tearing is low. Necking is a subjective process and is dependent on the measuring accuracy of the equipment and the skills of the experimenter. Occasionally, a curve 10% below the FLD related to the fracture is plotted and used as a safe FLD curve [26]. In Fig. 8, an FLD which is 10% lower in major strain than the EXP-FLD curve is also represented and is denoted by "EXP-FLD-10% below." As can be observed in Fig. 8, the predicted FLD is appropriately compatible with the experimental safe FLD.

5. Conclusions

In the present work, GTN damage model parameters were identified through inverse method for an IF-steel using RSM–CCD. Using the optimized values of the GTN model factors ($f_0 = 0.0002$, $f_N = 0.0106$, $f_c = 0.0134$, $f_f = 0.0216$, $\varepsilon_p = 0.1$ and $S_N = 0.1$) and based on RSM-CCD, the FLD of the specimen steel was predicted and was found to be in good agreement with the experimental diagram.

The correct identification of the GTN damage model parameters resulted in an appropriate analysis of formability. Therefore, the evaluation and identification of correct GTN model parameters values based on RSM are recommended.

References

[1] F. Ozturk and D. Lee, Experimental and numerical analysis of out-of-plane formability test, *J. Mater. Process. Technol.,* 170 (2005) 247-253.

[2] A. Menhaj, M. Abbasi, M. Sedighi and M. Ketabchi, A new concept in obtaining forming limit diagram of tailor welded blank, *J. Strain Analysis,* 46 (2011) 740-748..

[3] M. Aghaie-khafri, R. Mahmudi and H. Pishbin, Role of yield criteria and hardening laws in the prediction of forming limit diagrams, *Metall Mater Trans A,* 33 (2002) 1363-1371.

[4] S. E. Jones and P. P. Gillis, An analysis of biaxial stretching of a flat sheet, *Metall Mater Trans A,* 15 (1984) 133-138.

[5] C. Zhiying and D. Xianghuai, The GTN damage model based on Hill'48 anisotropic yield criterion and its application in sheet metal forming, *Comp. Mater. Sci.,* 44 (2009) 1013-1021.

[6] M. Brunet, F. Morestin and H. Walter, Damage identification for anisotropic sheet-metals using a non-local damage model, *Int. J. Damage. Mech.,* 13 (2004) 35-57.

[7] M. Abbasi, M. Ketabchi, H. Izadkhah, D. F. Haghshenas and A. N. Aghbash, Identification of GTN model parameters by application of response surface methodology, *Procedia Eng.,* 10 (2011) 415-420.

[8] M. Springmann and M. Kuna, Determination of ductile damage parameters by local deformation fields: measurement and simulation, *Arch. Appl. Mech.,* 75 (2006) 775-797.

[9] M. Brunet, S. Mguil and F. Morestin, Analytical and experimental studies of necking in sheet metal forming proc-

esses, *J. Mater. Process. Technol.,* 80-81 (1998) 40-46.
[10] L. Fratini, A. Lombardo and F. Micari, Material characterization for the prediction of ductile fracture occurrence: an inverse approach, *J. Mater. Process. Technol.,* 60 (1996) 311-316.
[11] G. B. Broggiato, F. Campana and L. Cortese, Identification of material damage model parameters: an inverse approach using digital image processing, *Meccanica*, 42 (2007) 9-17.
[12] D. C. Montgomery, *Design and analysis of experiments*, John Wiley & Sons, New York, USA (2006).
[13] M. Abbasi, B. Bagheri, M. Ketabchi and D. F. Haghshenas, Application of response surface methodology to drive GTN model parameters and determine the FLD of tailor welded blank, *Comp. Mater. Sci.,* 53 (2012) 368-376.
[14] A. L. Gurson, Continuum theory of ductile rupture by void nucleation and growth. Part I: yield criteria and flows rules for porous ductile media, *J. Eng. Mater. Technol*., 99 (1977) 2-15.
[15] A. K. Gupta and D. R. Kumar, Formability of galvanized interstitial-free steel sheets, *J. Mater. Process. Technol.,* 172 (2006) 225-237.
[16] ASTM Standards, Standard test methods for tension testing of metallic materials, ASTM E8-E8M, 2009.
[17] Abaqus/6.9 Software, Abaqus Analysis User's Manual (6.9), Porous metal plasticity, 2009.
[18] M. Abbasi, *Analysis of wrinkling and tearing of tailor welded blank during deep drawing process*, Ph. D. Thesis, Amirkabir University of Technology, Tehran, Iran (2011).
[19] Abaqus/6.9 Software, Dassault Systèmes Simulia Corp., Providence, RI, USA (2009).
[20] Z. Chen and X. Dong, The GTN damage model based on Hill'48 anisotropic yield criterion and its application in sheet metal forming, *Comp. Mater. Sci.,* 44 (2009) 1013-1021.
[21] J. Rojek, E. Onate and E. Postek, Application of explicit FE codes to simulation of sheet and bulk metal forming processes, *J. Mater. Process. Technol.,* 80-81 (1998) 620-627.
[22] D. Banabic, H. J. Bunge, K. Pöhlandt and A. E. Tekkaya, *Formability of metallic materials*, Springer-Verlag, Berlin, Germany (2000).
[23] A. Seireg, *Friction and lubrication in mechanical design*, Mechanical Engineering Series, Marcel Dekker Pub. (1998).
[24] M. A. Shafaat, M. Abbasi and M. Ketabchi, Investigation into wall wrinkling in deep drawing process of conical cups, *J. Mater. Process. Technol.* (2011), DOI: 10.1016/j.jmatprotec.2011.05.026.
[25] N. Amjadi and A. Shirzadi, Unit commitment using a new integer coded genetic algorithm, *Eur. T. Electr. Power,* 19 (2009) 1161-1176.
[26] W. F. Hosford and R. M. Caddell, *Metal forming-mechanics and metallurgy*, Cambridge University Press, Cambridge (2007).

Mahmoud Abbasi is currently a Ph.D student at Amirkabir University of Technology (AUT), Iran. He received his B.S. and M.S. degrees from the renowned University in Materials Science and Engineering. At present, his major field of study is material characterization and metal forming.

Mostafa Ketabchi received his B.S. and M.S. degrees in Materials Science and Engineering from Sharif University, Iran. After obtaining his Ph.D degree in Metal Forming from Tohoko University, Japan, he joined Amirkabir University of Technology as an academic staff. He has several published papers in ISI journals and proceedings. His main field of study is metal forming processes. Thermo-mechanical treatments and material characterization are his other areas of interest.